Relaxor nature in lead-free $Sr_5LaTi_3Nb_7O_{30}$ tetragonal tungsten bronze ceramics

Xiao Li Zhu, Kun Li, Muhammad Asif Rafiq, Xiao Qiang Liu, and Xiang Ming Chen'

Citation: Journal of Applied Physics **114**, 124102 (2013); doi: 10.1063/1.4822025
View online: http://dx.doi.org/10.1063/1.4822025
View Table of Contents: http://aip.scitation.org/toc/jap/114/12
Published by the American Institute of Physics

Relaxor nature in lead-free $Sr_5LaTi_3Nb_7O_{30}$ tetragonal tungsten bronze ceramics

Xiao Li Zhu,[1,2] Kun Li,[1] Muhammad Asif Rafiq,[2] Xiao Qiang Liu,[1] and Xiang Ming Chen[1,a)]
[1]*Department of Materials Science and Engineering, Laboratory of Dielectric Materials, Zhejiang University, 38 Zheda Road, Hangzhou 310027, China*
[2]*Department of Materials and Ceramic Engineering, Centre for Research in Ceramics and Composite Materials, CICECO, University of Aveiro, 3810 193 Aveiro, Portugal*

(Received 18 July 2013; accepted 9 September 2013; published online 24 September 2013)

Lead-free tetragonal tungsten bronze $Sr_5LaTi_3Nb_7O_{30}$ ceramics were prepared and the correlation of the relaxor nature and crystal structure was studied using dielectric spectroscopy and powder X-ray diffraction. Three dielectric relaxations were observed below the deviation temperature $T_D \sim 330$ K. Relaxation I and II followed the Vogel-Fulcher law with the freezing temperatures of 189 K and ~90 K. Low temperature relaxation III, which was first observed in filled tungsten bronze, followed well the Arrhenius law. Dielectric response becomes static below 50 K. Polarization-field (P-E) hysteresis loops were evaluated from 183 K to 298 K. P_r value of 0.41 μC/cm^2 was observed at 183 K. Deviation of lattice parameter c from the linear contraction and increasing of tetragonality (c/a ratio) were observed below T_D, reflecting the structure change during the formation of polar nanoregions and the following freezing process. Opposite tendency was observed below 100 K for all the lattice parameters, corresponding to relaxation III. Generally, the main dielectric relaxation I and II were attributed to flipping and breathing of polar nanoregions along c axis, while the concerted rotations of the oxygen octahedra in the ab plane were suggested as the origin of relaxation III. © *2013 AIP Publishing LLC*. [http://dx.doi.org/10.1063/1.4822025]

I. INTRODUCTION

High and broad maxima in temperature dependence of dielectric constant (ε') and dielectric loss (ε'') and their shift to higher temperature with increasing frequency form the typical features of relaxor ferroelectrics. Since the first report of about half a century ago, relaxor ferroelectric materials have attracted high attention and been studied intensively due to not only their potential technical applications in piezoelectric devices and microelectronics, but also their peculiar physics of partially disordered materials.[1–4] The particular structural, dielectric, and electromechanical behaviors of relaxor ferroelectrics are generally related to the presence of polar nanoregions above and below the maximum temperature of permittivity (T_m). Since most of the relaxor ferroelectrics with potential applications are lead-based single crystals and ceramics with perovskite structure,[1,2] understanding of the polar nanoregions in relaxor ferroelectrics are mainly based on the study of compounds with perovskite structure. In perovskite relaxor ferroelectrics, the polar nanoregions are related to chemical disorder of cations with different valence in the B-sites,[2,3] while in lead-based perovskite relaxor ferroelectrics, the dynamic Pb-disorder plays a more dominant role than the B-site disorder.[4–6] The increased need of environmental friendly lead-free dielectric and microelectric materials promote the search, development and study of new lead-free ferroelectrics and relaxor ferroelectrics. However, the mechanism of relaxor behavior and the origin of the polar nanoregions are much less understood in lead-free relaxor ferroelectrics, especially the tetragonal tungsten bronze relaxor ferroelectrics, which consist of one of the most important classes of dielectrics just next to the perovskites.

The tungsten bronze structure, $(A1)_2(A2)_4C_4(B1)_2(B2)_8O_{30}$, consists of a complex array of BO_6 octahedra sharing corners. The octahedra are linked by their corners in such a way that three different types of tunnels running right through the structure parallel to the c-axis in the unit cell of tungsten bronze structure, which provide high degrees of freedom for manipulation of the structure allowing more compositional flexibility than perovskite structure.[7,8] Normally, the tetragonal ($A1$) and the pentagonal ($A2$) tunnels are occupied by alkali, alkaline earth, and rare-earth cations. The smallest triangular C interstice is empty in many tungsten bronzes, and can be filled by smaller cations like Li^+.

Recently, the relaxor and ferroelectric behavior have been noticed in a series of ternary and quaternary systems with filled tetragonal tungsten bronze structure, including $A_6B_2B'_8O_{30}$ (A = Sr, Ba, or Pb; B = Ti, Zr, or Hf; B′ = Nb or Ta) [Refs. 9 11], $Ba_6M^{3+}Nb_9O_{30}$ (M^{3+} = Ga, Sc, or In) [Refs. 12 and 13], $M_4R_2Ti_4Nb_6O_{30}$ [Refs. 14 20], and $M_5RTi_3Nb_7O_{30}$ [Refs. 21 25] (M = Ba and Sr; R represents the larger rare earth ions ranging from La to Dy and also Bi). In the ternary $A_6B_2B'_8O_{30}$ system, both Ti^{4+} and Nb^{5+} were considered to be ferroelectrically active cations.[9] In $Ba_6M^{3+}Nb_9O_{30}$ system, dipole freezing behavior is observed and the dipole stability increases with increasing M^{3+} cation size as a result of increased tetragonality of the unit cell.[13] The relaxor and ferroelectric nature in the quaternary $M_4R_2Ti_4Nb_6O_{30}$ systems are generally dominated by the A-site cations, especially the radius difference (ΔR) between the ions

a)Author to whom correspondence should be addressed. Electronic mail: xmchen59@zju.edu.cn

on the *A*1 (tetragonal) and the *A*2 (pentagonal) sites.[19,20] Larger ΔR increases the driving force of the transformation of an incommensurate tilted structure to a commensurate superstructure, which associated with the normal ferroelectric transition.[15,16] For the relaxor behavior in the quaternary tungsten bronzes, some peculiarities in the dielectric response, relaxation and crystal lattice dynamics have been revealed in $Sr_4La_2Ti_4Nb_6O_{30}$, which was claimed more alike to dipolar glasses than lead-based perovskite.[18] However, the second order phase transition was reported for relaxor ferroelectric $Ba_5LaTi_3Nb_7O_{30}$.[24] The nature of the relaxor behavior in the quaternary tungsten bronzes and its relation with compositions are not yet clear. Therefore, intensive study in relaxor ferroelectrics with tungsten bronze structure is necessary for more clear understanding of the nature and origin of the polar nanoregions in these materials.

The dielectric and ferroelectric properties in $Sr_5RTi_3Nb_7O_{30}$ (R = La, Nd, Sm, and Eu) ceramics were reported in the authors' previous work,[25] where the effects of radius difference in A site were discussed and $Sr_5LaTi_3Nb_7O_{30}$ showed relaxor behavior due to smaller ΔR. However, the relaxor nature in $Sr_5LaTi_3Nb_7O_{30}$ ceramics has not been well understood. The present paper reports a comprehensive study of the dielectric relaxation response, ferroelectric property, and the crystal structure in $Sr_5LaTi_3Nb_7O_{30}$ ceramics. Nature and origin of the relaxor behavior are discussed intensively associated with the variation in the crystal structure.

II. EXPERIMENT

$Sr_5LaTi_3Nb_7O_{30}$ ceramics were prepared by a standard solid-state reaction and sintering process, using reagent-grade $SrCO_3$ (99.95%), La_2O_3 (99.99%), TiO_2 (99.5%), and Nb_2O_5 (99.99%) powders as the raw materials. The weighed raw materials were mixed by ball milling with zirconia media in ethanol for 24 h. The mixtures were calcined in high-purity alumina crucibles at 1200 °C in air for 3 h followed by a second grinding to reach a homogeneous granulometric distribution. Adding with organic binders (8 wt. % polyvinyl alcohol), the reground powders were pressed into cylindrical compacts of 12 mm in diameter and around 2 mm in thickness under the pressure of about 98 MPa. The disks were sintered at 1250 1350 °C in air for 3 h to yield the dense ceramics.

The crystal structure was identified by powder XRD analysis with Cu Ka radiation. At room temperature, the XRD data were collected over the 2θ range of 8° to 130° with a step size of 0.02° (D/max 3B, Rigaku Co., Tokyo, Japan). XRD data at temperatures between 93 and 573 K were collected over the 2θ range of 9° to 100° with a step size of 0.03° (Philips MPD, Amsterdam, the Netherlands) with a low temperature chamber (Anton Paar TTK-450, Graz, Austria). The FULLPROF program was used for Rietveld structural refinement.[26] Dielectric properties in the range of 128 K to 573 K were measured with a broadband dielectric spectrometer (Turkey Concept 50; Novocontrol Technologies, Hundsangen, Germany) over a frequency range of 1 Hz to 10 MHz). Low temperature dielectric properties were collected over a frequency range of 100 Hz to 1 MHz and from room temperature cooling to 10 K using a homemade system with an Agilent E4980A Precision LCR meter (Santa Clara, CA, USA) and cooling system (ARS-2HW Compressor, Advanced Research Systems, Inc., Macungie, PA, USA). The temperature is measured using a Digital temperature controller (Model 9650, Scientific Instruments, Inc., Skokie, IL, USA) via a platinum resistance thermometer mounted directly on the ground electrode of the sample fixture. The temperature controller and Agilent E4980A are controlled with computer software. P-E hysteresis loops were evaluated from 183 K to 298 K at 10 Hz by a Precision Materials Analyzer (RT Premier II, Radiant Technologies, Inc., NM).

TABLE I. Refined atomic positions and thermal parameter of $Sr_5LaTi_3Nb_7O_{30}$ in tetragonal space group *P*4/*mbm*. *a* 12.3324(9) Å and *c* 3.8780(5) Å.

	x	y	z	B_{iso}(Å^2)	Occupation	Wyckoff
La1/Sr1	0	0	0	1.39(5)	0.46/0.54	2*a*
La2/Sr2	0.1706(1)	0.6706(1)	0	4.32(7)	0.02/0.98	4*g*
Ti1/Nb1	0	0.5	0.5	2.90(6)	0.3/0.7	2*c*
Ti2/Nb2	0.0763(1)	0.2149(1)	0.5	1.49(3)	0.3/0.7	8*j*
O1	0	0.5	0	6.4(6)	1	2*d*
O2	0.2759(6)	0.7759(6)	0.5	3.44(16)	1	4*h*
O3	0.0738(7)	0.2076(6)	0	3.68(16)	1	8*j*
O4	0.3391(5)	0.0075(5)	0.5	2.9(2)	1	8*j*
O5	0.1330(6)	0.0629(7)	0.5	3.9(2)	1	8*j*

III. RESULTS AND DISCUSSION

A. General observations

Room-temperature XRD indicated the single tetragonal tungsten bronze phase for $Sr_5LaTi_3Nb_7O_{30}$ ceramics. The XRD spectra were refined in the space group *P*4/*mbm* (No. 127) using the Rietveld method. The final parameters of the refined crystal structure are summarized in Tables I and II. Cation distribution in *A* sites slightly deviates from the expected ratio of 1:1 Sr^{2+}/La^{3+} in *A*1 site and 4 Sr^{2+} in *A*2 site, with a ratio of $0.92La^{3+}$: $1.08Sr^{2+}$ in *A*1 site, while $3.92Sr^{2+}$: $0.08La^{3+}$ in *A*2 site.

The overall dielectric response of $Sr_5LaTi_3Nb_7O_{30}$ is similar to that of other tungsten bronze compounds with relaxor behavior.[13,18,24] As shown in Figure 1, in the temperature range from 128 K to 573 K, diffuse peaks of the complex dielectric permittivity, $\varepsilon = \varepsilon' - i\varepsilon''$, and the loss factor, $\tan\delta = \varepsilon'/\varepsilon''$, move towards higher temperatures with increasing frequency. Dielectric dispersion of the main relaxation takes place in broad temperature and frequency regions both below and

TABLE II. Bond Lengths in $Sr_5LaTi_3Nb_7O_{30}$.

Bond lengths (Å)		Bond lengths (Å)	
La1/Sr1 O3	2.717(8) × 4	Ti1/Nb1 O1	1.93902(3) × 2
La1/Sr1 O5	2.656(5) × 8	Ti1/Nb1 O4	1.986(7) × 4
		Ti2/Nb2 O2	1.972(8) × 1
La2/Sr2 O1	2.9754(15) × 1	Ti2/Nb2 O3	1.9414(4) × 2
La2/Sr2 O2	2.671(5) × 2	Ti2/Nb2 O4	1.847(7) × 1
La2/Sr2 O4	2.796(5) × 4	Ti2/Nb2 O5	2.002(9) × 2

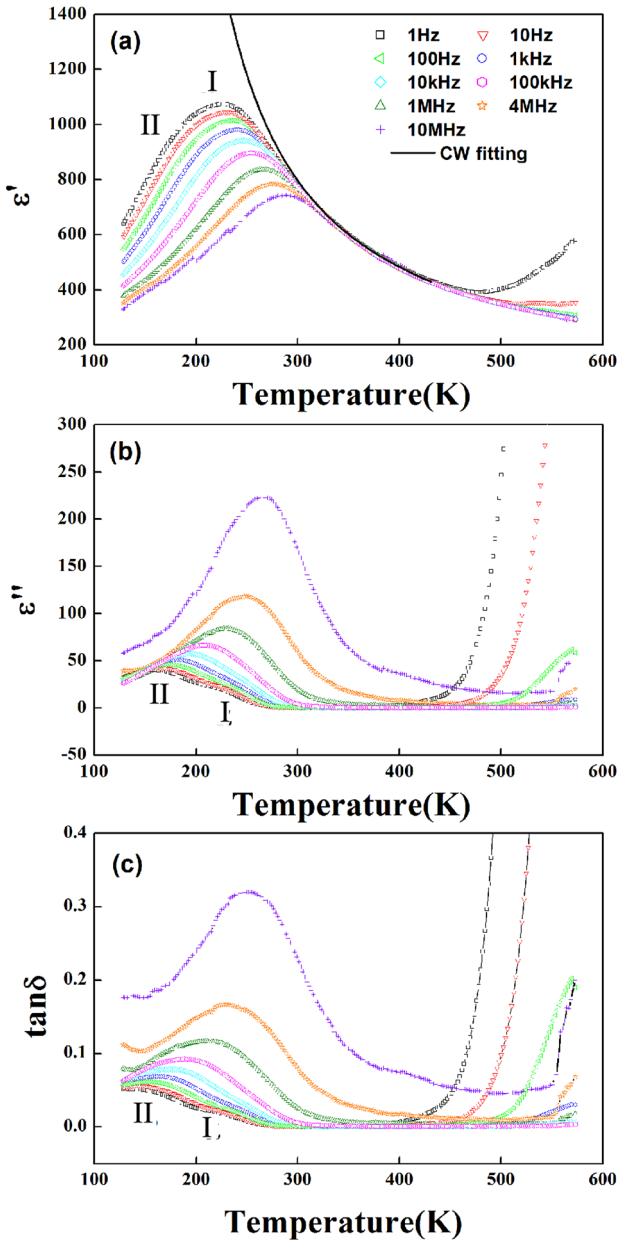

FIG. 1. Temperature dependence of (a) dielectric constant ε', (b) dielectric loss ε'', and (c) dielectric loss factor tanδ of $Sr_5LaTi_3Nb_7O_{30}$ in the temperature range of 128 K to 573 K and frequency range between 1 Hz and 10 MHz.

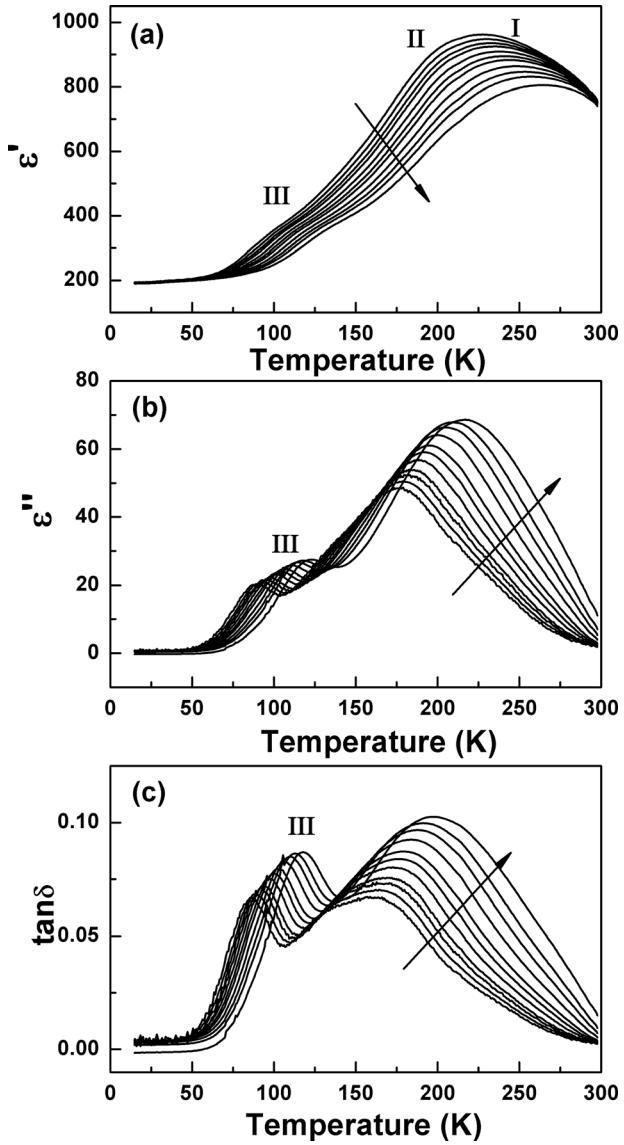

FIG. 2. Temperature dependence of (a) dielectric constant ε', (b) dielectric loss ε'', and (c) dielectric loss factor tanδ of $Sr_5LaTi_3Nb_7O_{30}$ in the temperature range of 10 K to 300 K from 398 Hz to 1 MHz.

above the permittivity maximum temperature T_m. This dielectric relaxation appears around 250 K and tends to split into two relaxation regions (relaxation I for the higher temperature region, while relaxation II for the lower temperature region) at lower frequency, which is more obvious in the dielectric loss curves. In order to get more information, dielectric measurement was performed from room temperature to 10 K in the frequency range of 398 Hz $\sim$ 1 MHz, and the results are shown in Figure 2. Except for the overlapped relaxations I and II, one more relaxation, relaxation III, can be clearly seen in the $\varepsilon''(T)$ and tan$\delta(T)$ curves around 100 K, showing a Debye-like dispersion. This low temperature relaxation III is observed in filled tungsten bronze ceramics for the first time. At temperature lower than 50 K, the dielectric permittivity becomes almost stable with temperature and frequency.

The ferroelectric hysteresis loops were measured on cooling from room temperature down to 183 K. As shown in Figure 3(a), the hysteresis loop exhibits almost linear behavior at room temperature, while slim *P-E* hysteresis loops can be observed with the gradually increasing remnant polarization (P_r) on cooling cross the T_m region. A remnant polarization (P_r) of 0.41 μC/cm^2 and the corresponding coercive field (E_c) of 3.56 kV/cm are obtained at 183 K. The above characteristics of the *P-E* hysteresis loops for $Sr_5LaTi_3Nb_7O_{30}$ indicate the typical behavior similar to the perovskites relaxor ferroelectrics, where the nanoregions can be oriented with the sufficiently high electric fields leading to large polarization, while on removing the field most of these domains reacquire their random orientations resulting in a relatively small P_r. The small P_r is evidence for the presence of some degree of cooperative freezing of dipolar (or nanoregions) orientations.[2]

According to the study of the contribution of electrical conductivity, dielectric permittivity, and domain switching

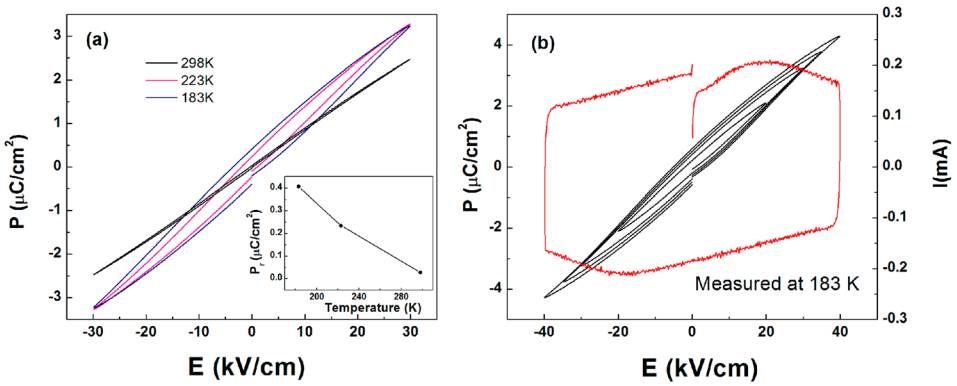

FIG. 3. (a) Polarization electric field (P E) loops at different temperatures. (b) P E loops with different applied electric field and current electric field (I E) curve at 183 K.

in ferroelectric I-E loops, the current from dielectric with no ferroelectric property is almost a constant value, while for the contribution from the domain switching, the current peak appears before the maximum electric field.[27] The current peak exhibits in the *I-E* loop at 183 K and 20 kV/cm (see Figure 3(b)), suggesting the existence of domain switching in the $Sr_5LaTi_3Nb_7O_{30}$ ceramics at low temperature.

B. Analysis of dielectric data

Temperature dependences of ε' follow the Curie-Weiss (CW) law above ~330 K for all the applied frequencies from 1 Hz to 10 MHz with the extrapolated critical temperature $T_{CW} \approx 146$ K and the Curie-Weiss constant $C \sim 1.22 \times 10^5$ K. The dielectric constant deviates from the CW law below 330 K, which is called the deviation temperature T_D,[28,29] and indicates the diffuse behavior. The diffuse behavior of dielectric constant from T_m to T_D can be described by a modified Curie Weiss law[30,31]

$$\ln(1/\varepsilon' - 1/\varepsilon'_m) = \gamma \ln(T - T_m) + C', \quad (1)$$

where ε'_m is the dielectric constant at T_m, C' is the Curie constant, γ is called a diffusion exponent, ranging from 1(a normal ferroelectric) to 2(an ideal relaxor ferroelectric). $\ln(1/\varepsilon'\text{-}1/\varepsilon'_m)$ as a function of $\ln(T\text{-}T_m)$ is plotted for all the applied frequencies from 1 Hz to 10 MHz. A linear relationship is observed for all the applied frequencies in the temperature range from T_m to T_D. The γ values obtained from fitting of data at different frequencies vary slightly from 1.91 to 1.93, indicating quite strong diffuse nature for the relaxor behavior in $Sr_5LaTi_3Nb_7O_{30}$. The measured data and linear fits for 1 Hz and 4 MHz are shown in Figure 4.

Maximum temperatures T_m of the dielectric relaxations obtained from the dielectric constant ($\varepsilon'(T)$) and loss ($\varepsilon''(T)$) curves at different frequencies are plotted in Figure 5. For the main relaxation, T_m data obtained from both the $\varepsilon'(T)$ and loss $\varepsilon''(T)$ curves follow well the Vogel-Fulcher expression which was first adopted by Viehland in the study of relaxor behavior in $PbMg_{1/3}Nb_{2/3}O_3$.[32] The Vogel-Fulcher model mainly describes a temperature dependence of relaxation times and probes the thermal activated process of the dipolar response in relaxor ferroelectrics. The Vogel-Fulcher Eq. (2) is simply a modified Arrhenius expression, which includes the increasing interaction between random local dipolar regions:

$$f = f_0 \exp\left(-E_a/k(T_m - T_{VF})\right), \quad (2)$$

where f is the applied ac field frequency (Hz); f_0 is the fundamental attempt or limiting response frequency of the dipoles (Hz); E_a is the activation energy of local polarization; T_m is the temperature (K) of permittivity maximum at frequency f; T_{VF} is the characteristic Vogel-Fulcher temperature (usually described as the static freezing temperature (K)); and k is Boltzmann's constant (1.381×10^{-23} J/K). Fitting parameters are obtained as $T_{VF} \sim 189$ K, $E_a \sim 0.088$ eV, $f_0 \sim 0.449$ THz for the $\varepsilon'(T)$ data and $T_{VF} \sim 95.62$ K, $E_a \sim 0.141$ eV, $f_0 \sim 0.185$ THz for the $\varepsilon''(T)$ data. Since the relaxations I and II are not well separated, only one T_m value can be obtained from the $\varepsilon'(T)$ and $\varepsilon''(T)$ curves. According to the results of Vogel-Fulcher fittings, it is likely that the T_m values from $\varepsilon'(T)$ indicate the freezing process of relaxation I, while T_m values from $\varepsilon''(T)$ reflect the behavior of relaxation II. Vogel-Fulcher fitting for the T_m data of the relaxation III obtained from $\varepsilon''(T)$ curves leads to a minus T_{VF}, which is

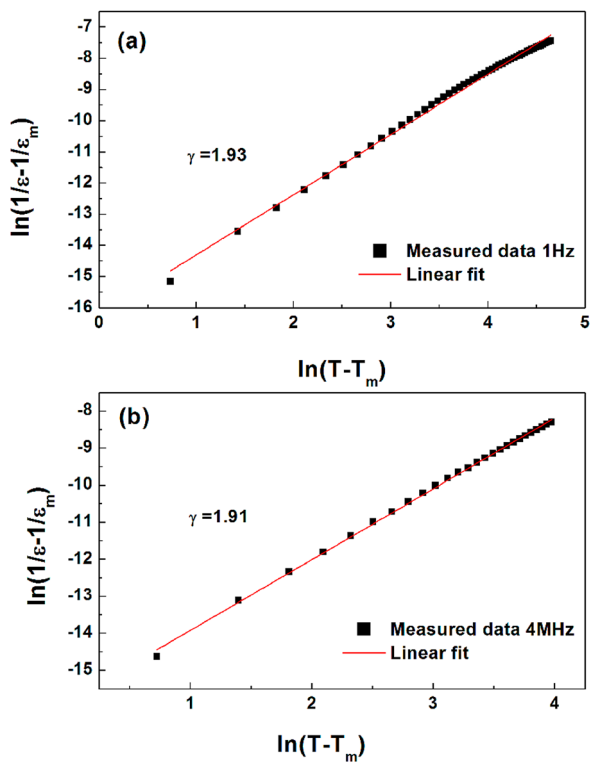

FIG. 4. $\ln(1/\varepsilon' \ 1/\varepsilon'_m)$ as a function of $\ln(T \ T_m)$ at 1 Hz (a) and 4 MHz (b).

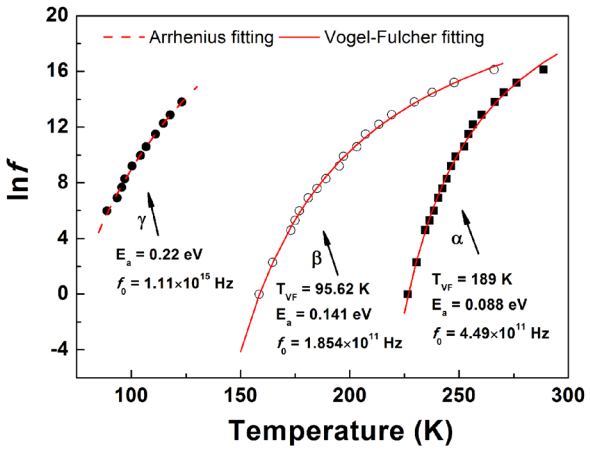

FIG. 5. Relations between applied frequencies and T_m estimated from $\varepsilon''(T)$ curves and $\varepsilon'(T)$ curves, while solid square for the relaxation α from $\varepsilon'(T)$ curves, and open circle for relaxation β and solid circle for relaxation γ from $\varepsilon''(T)$ curves. Solid red lines show the Vogel Fulcher fitting results for relax ation α and β, and dashed red line shows the Arrhenius fitting result for relaxation γ.

not physically sensible. Fitting to the Arrhenius Law [$f = f_0 \exp(-E_a/kT_m)$] gives $E_a \sim 0.22\,\text{eV}$, $f_0 \sim 1.11 \times 10^{15}\,\text{Hz}$. Therefore, relaxation III shows an Arrhenius behavior.

The dielectric data are plotted in the frequency domain for temperatures around relaxations I and II in Figure 6. Due to the limit range of the applied frequency, it is not allowed to get peak values from the $\varepsilon''(f)$ curves. An alternative solution was applied to get the mean relaxation time by fitting the $\varepsilon''(f)$ data (Figure 6(a)) to the modified Debye Equation

$$\varepsilon^* = \varepsilon' - i\varepsilon'' = \varepsilon_\infty + (\varepsilon_s - \varepsilon_\infty)/[1 + (i\omega\tau)^{1-\alpha}], \quad (3)$$

where ω is the frequency, τ is the mean relaxation time, ε_s and ε_∞ are the low- and high-frequency values of ε', respectively, and α is a measure of the distribution of relaxation time. For a typical Debye relaxation, α is zero. The fitting parameters of α and τ at temperatures around the dielectric relaxation are plotted in Figure 7(a). The dielectric relaxation shows a multi-dispersive nature in the present ceramics with α varying from 0.36 to 0.92, where τ increases from 4.68×10^{-10} s to 0.024 s with decreasing temperature. This means the relaxation in $Sr_5LaTi_3Nb_7O_{30}$ disperses in a wide frequency range from the magnitude of GHz at ~300 K to the range of kHz at ~150 K. The mean relaxation time τ can also be fitted to the Vogel-Fulcher law

$$\tau = \tau_0 \exp\left(E_a/k(T - T_{VF})\right). \quad (4)$$

Here, τ_0 is reciprocal of f_0 in Eq. (2). The fitting results are 83.2 K, 0.123 eV, and 2.43×10^{12} Hz for $T_{VF}(\varepsilon''(f))$, E_a and $f_0(1/\tau_0)$, which are in comparison to the Vogel-Fulcher fitting results obtained from the peak value of ε''(T) curves. Figure 7(b) shows temperature dependence of the mean relaxation

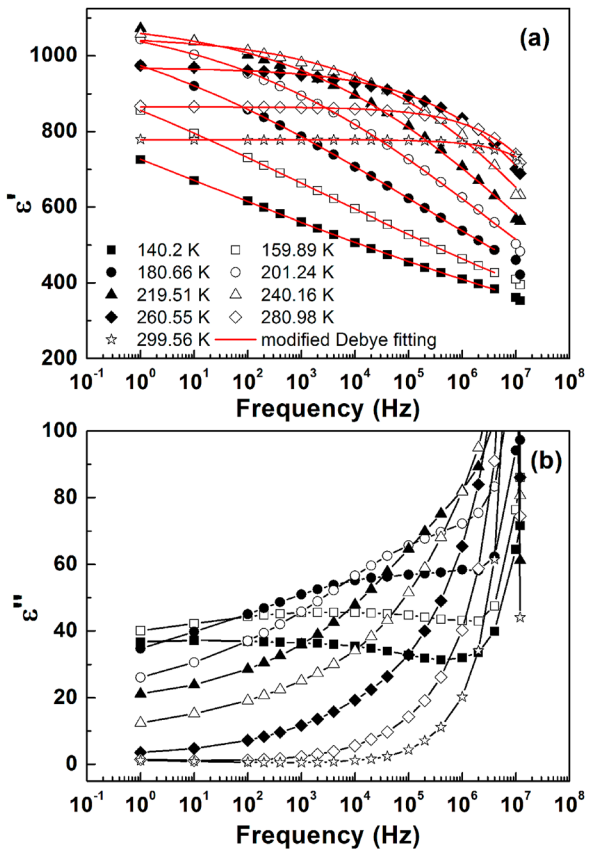

FIG. 6. Frequency dependences of the dielectric constant (a) and loss (b) of $Sr_5LaTi_3Nb_7O_{30}$ at selected temperatures. Solid red lines in (a) are the results of modified Debye fitting.

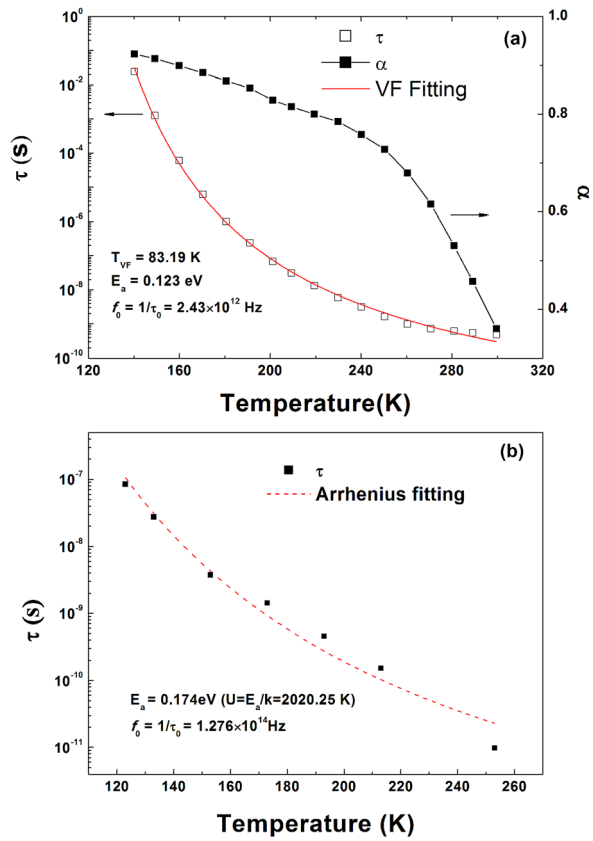

FIG. 7. (a) Temperature dependences of mean relaxation time τ and α, obtained from the modified Debye fittings for $Sr_5LaTi_3Nb_7O_{30}$. (b) Temperature dependences of mean relaxation time τ, obtained from the modified Debye fittings for $Sr_5LaTi_3Nb_7O_{30}$ [Ref. 37]. Solid red line: Vogel Fulcher fitting; dashed red line: Arrhenius fitting.

time of $Sr_4La_2Ti_4Nb_6O_{30}$ obtained from the modified Debye fitting to the $\varepsilon'(f)$ data (reported in authors' previous work[33]), which follows the Arrhenius law. The fitting results in Figure 7(b) are consistent with that reported by Bovtun *et al.*,[18] indicating that the mean relaxation times obtained from the modified Debye fitting are reliable.

As predicted by the theory of relaxor ferroelectrics, the dielectric loss peak in $\varepsilon''(f)$ curve associated with the dipolar response should become infinitely broad (flat) at the static freezing temperature. A symmetric loss peak with the Debye response can be fitted to a Gaussian distribution of relaxation times.[13] Due to the multi-dispersive nature of the dielectric relaxation, the frequency dependence of the dielectric loss data in $Sr_5LaTi_3Nb_7O_{30}$ (Figure 6(b)) indicates a high degree of asymmetry. This asymmetric dielectric loss data can be fitted to the empirical two-exponent model of Jonscher's universal dielectric response[34] (UDR) with the following relationship:

$$\varepsilon'' = \frac{1}{(f/f_p)^{m} + (f/f_p)^{1-n}}, \tag{5}$$

where f_p is the relaxation frequency (obtained from reciprocal of the mean relaxation time τ), and m and (1-n) are the frequency exponents of $\varepsilon''(f)$ below and above f_p, respectively, with the conditions $0 \le m,\ n \le 1$. For the Debye response, $m = (1\text{-}n) \le 1$. In the applied frequency range (1 Hz $\sim$ 10 MHz), dielectric loss peaks of the $\varepsilon''(f)$ curves can only be obtained at temperatures from 151.27 K to 180.66 K. Fits to UDR model of dielectric loss data in this temperature range are shown in Figure 8(a). The temperature dependence of the gradient m on the low frequency side is shown in Figure 8(b) and indicates a steady decrease with decreasing temperature. Extrapolation of the m data to zero gives the dipole freezing temperature $T_{UDR} \sim 91.5$ K, in comparison to $T_{VF}(\varepsilon''(T))$ of 95.6 K and $T_{VF}(\varepsilon''(f))$ of 83.2 K. Therefore, the high temperature relaxation observed in the $\varepsilon''(T)$ curves is mainly reflect the feature of relaxation II, and the freezing temperature is around 90 K using the above three different approaches.

Summarizing, three dielectric relaxations are observed in the temperature range from 10 K to 573 K, including two overlapping relaxations I and II, and a Debye-like relaxation III. Relaxations I and II follow well the Vogel-Fulcher law with different freezing temperature T_{VF} and activation energy E_a, possibly suggesting two relaxation contributions in $Sr_5LaTi_3Nb_7O_{30}$. Relaxation III follows well the Arrhenius Law. Origin of these two relaxation contributions and nature of relaxation III will be discussed in more details below.

C. Temperature dependence of crystal structure

XRD was measured at various temperatures from 93 K to 573 K, in order to investigate any possible change in the crystal structure of $Sr_5LaTi_3Nb_7O_{30}$. The obtained spectra are shown in Figure 9, and there is no evidence of macroscopic symmetry change in $Sr_5LaTi_3Nb_7O_{30}$. Only slight shift of the XRD peaks can be observed with decreasing temperature. All the data were refined in the tetragonal space group *P*4/*mbm*. The refined parameters for different temperatures are listed in

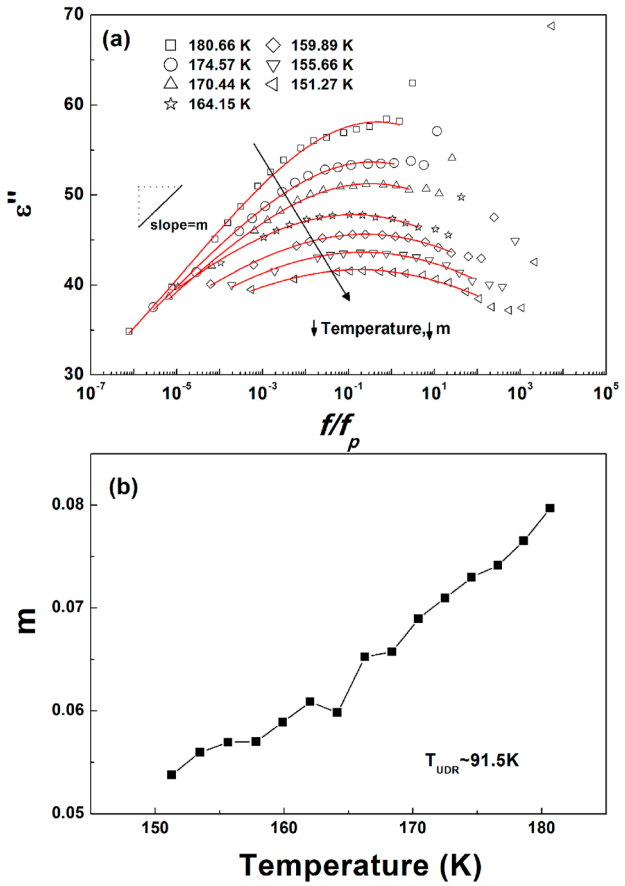

FIG. 8. Dielectric loss peaks fitted to Jonscher's two exponent model (a); gradient m for $\varepsilon''(f)$ at $f < f_p$ (b).

Table III. As shown in Figure 10, lattice parameter a (*ab* plane) and the unit cell volume exhibit linear contractions on cooling and reach a minimum value around 100 K (Figures 10(a) and 10(c)). The c-axis data (Figure 10(b)) deviate from the expected linear behavior at much higher temperature around 330 K (T_D'), and then the contraction rate slows down gradually with decreasing temperature below T_D' and reaches a minimum value also around 100 K ($T_{c/a}$). The variation of tetragonality (c/a ratio) with temperature is plotted in Figure 10(d), where the c/a ratio is quite stable above T_D', while

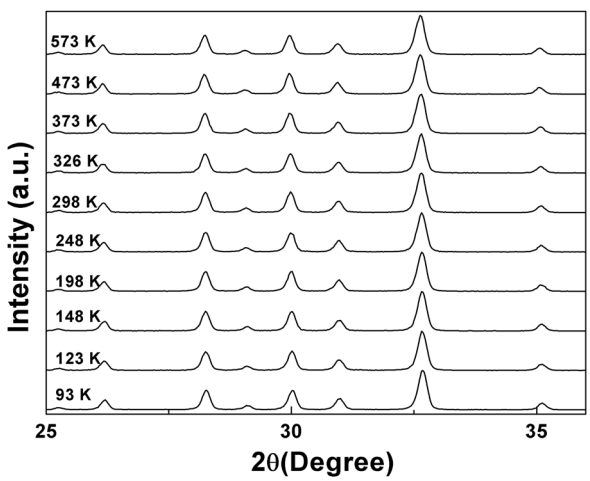

FIG. 9. XRD curves of $Sr_5LaTi_3Nb_7O_{30}$ from 93 K to 573 K.

TABLE III. Parameters of the Rietveld refinement for $Sr_5LaTi_3Nb_7O_{30}$ at different temperatures.

T(K)	93	98	123	148	173	198	223	248
R_p(%)	11.0	10.9	10.5	10.8	11.0	10.5	10.5	10.4
R_{wp}(%)	15.4	16.0	15.9	15.4	16.1	14.4	15.1	14.0
R_{exp}(%)	11.5	11.4	11.3	11.5	11.4	11.5	11.6	11.5
GOF	1.3	1.4	1.4	1.3	1.4	1.2	1.3	1.2
χ^2	1.795	1.975	1.979	1.814	1.972	1.577	1.719	1.472
T(K)	273	298	326	373	423	473	523	574
R_p(%)	10.3	10.8	11.0	10.4	10.7	10.8	10.5	10.8
R_{wp}(%)	14.4	15.2	15.8	13.6	14.3	14.7	14.6	15.0
R_{exp}(%)	11.5	11.6	11.6	11.7	11.8	11.8	11.8	11.9
GOF	1.2	1.3	1.3	1.2	1.2	1.2	1.2	1.2
χ^2	1.566	1.725	1.835	1.357	1.472	1.564	1.518	1.570

increases on cooling and reaches a maximum tetragonality around 100 K. $T_D' \sim 330$ K, which is dominated by the variation of *c*-axis data, is agree with the deviation temperature T_D of the $\varepsilon'(T)$ data, indicating the structural origin of the polar nanoregions.

Maximum crystallographic strain ($T_{c/a}$) was reported in $Ba_6M^{3+}Nb_9O_{30}$ (M^{3+} = Ga, Sc, or In), where only the *c*-axis data deviates from the expected linear behavior around the $T_{c/a}$ area, and was correlated to the freezing process of the dielectric relaxation.[13] Comparing the variation of lattice parameters in $Sr_5LaTi_3Nb_7O_{30}$ with that in $Ba_6M^{3+}Nb_9O_{30}$, several differences are found. The $T_{c/a} \sim 100$ K of $Sr_5LaTi_3Nb_7O_{30}$ are much lower than that in $Ba_6M^{3+}Nb_9O_{30}$. Moreover, two freezing temperatures are obtained for $Sr_5LaTi_3Nb_7O_{30}$ (189 K for relaxation I and ~90 K for relaxation II). If the $T_{c/a}$ value reflected the freezing temperature, there should be two critical temperatures in the *c/a* ratio-T curve. Around $T_{c/a}$ of $Sr_5LaTi_3Nb_7O_{30}$, all the lattice parameters show an extreme value, not only the *c*-axis data. The extreme temperature (~100 K) of the lattice parameters in $Sr_5LaTi_3Nb_7O_{30}$ is more consistent with the temperature range of relaxation III.

D. Nature and origin of relaxor behaviors

In relaxor ferroelectrics, deviation of the $\varepsilon'(T)$ curve from the Curie-Weiss behavior at temperature above T_m indicates the formation of polar nanoregions, and the deviation temperature T_D is also determined as the Burn's temperature.[28] In $Sr_5LaTi_3Nb_7O_{30}$, the high temperature dielectric constant follows the Curie-Weiss law until $T_D \sim 330$ K on cooling, suggesting the formation of polar nanoregions in $Sr_5LaTi_3Nb_7O_{30}$ below 330 K. Structural analysis in $Sr_5LaTi_3Nb_7O_{30}$ shows the deviation of lattice parameter *c* from the linear contraction and increasing of tetragonality (*c/a* ratio) below T_D, indicating some subtle structure change related to the formation of the polar nanoregions. It could be suggested that the subtle structure change in $Sr_5LaTi_3Nb_7O_{30}$ is the result of the increasing distortion of the oxygen octahedron on cooling, which could be the structure origin of the polar nanoregions.

The deviation degree can be defined by $\Delta T_m(f) = T_D - T_m(f)$. For instance, in lead-based perovskites relaxor PMN,

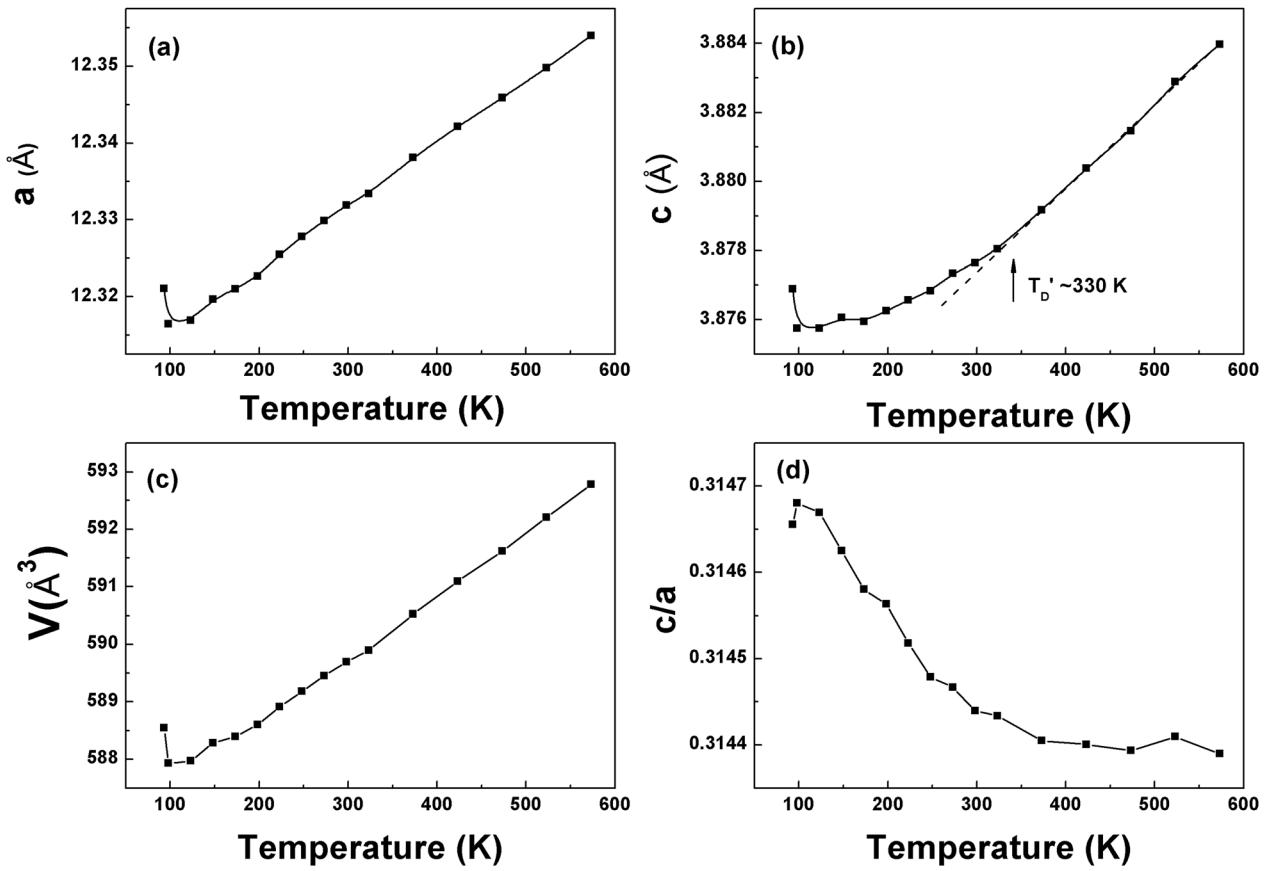

FIG. 10. Lattice parameters [(a) and (b)], unite cell volume (c), and tetragonality *c/a* ratio (d) as a function of temperature for $Sr_5LaTi_3Nb_7O_{30}$.

$\Delta T_m = 618$ K- (230 ~ 250 K) ≈ 380 K [Ref. 28], while for $(1-x)(K_{0.5}Na_{0.5})NbO_3$-$x(Ba_{0.5}Sr_{0.5})TiO_3$ (x = 005-0.2), ΔT_m (1 MHz) varies from 94 K to 191 K [Ref. 29]. In the case of $Sr_5LaTi_3Nb_7O_{30}$, ΔT_m decreases from ~105 K to ~40 K with increasing frequency from 1 Hz to 10 MHz, which is smaller compared with that in perovskite relaxors. It is likely that in tungsten bronze relaxors, the deviation temperature of dielectric constant from the CW law is lower than that in perovskite relaxors. In relaxor ferroelectrics, the deviation from the CW behavior indicates different interaction between polar nanoregions from that between the dipolar in a paraelectric phase. The lower deviation temperature and smaller ΔT_m value indicate the weaker interaction between the polar nanoregions in tungsten bronze relaxors.

According to Bovtun *et al.*,[18] the relationship between the Curie-Weiss temperature T_{CW}, freezing temperature T_{VF} and T_m reflects the interaction between the polar nanoregions. In case of lead-based perovskite relaxors with strong intercluster interaction, T_{CW} is much higher than T_{VF} and T_m. In the cases of doped incipient ferroelectrics and tungsten bronze relaxor $Sr_4La_2Ti_4Nb_6O_{30}$ with weak intercluster interaction, T_m is higher than T_{CW} and T_{VF}, which are close to each other. The situation of $Sr_5LaTi_3Nb_7O_{30}$ is similar to the latter ones: $T_m \sim 250\,K > T_{CW} = 146\,K \approx T_{VF} = (189\,K/\sim 90\,K)$, also indicating the weak interaction between the polar nanoregions and the relaxation nature between the dipolar glass and typical relaxor ferroelectrics.

In filled tungsten bronzes, the relaxor or ferroelectric behavior is dominated by the distortion of the oxygen octahedron forming the incommensurate tilted structure or commensurate superstructure, which associated with the radius difference (ΔR) between the $A1$ and $A2$ site cations.[15] In tungsten bronzes with large ΔR, like $M_4R_2Ti_4Nb_6O_{30}$ (M = Sr, Ba; R = Nd, Sm, Eu), ferroelectric transition occurs at the transition temperature of the incommensurate to commensurate structure. The driving force for the commensurate tilting decreases with decreasing ΔR, then incommensurate structure stays in tungsten bronze with small ΔR, indicates the relaxor behavior. Dynamics of both the polar nanoregions and the incommensurate tilting are considered to be responsible for the relaxor behavior below T_D.

The two overlapping relaxations I and II are possibly due attributed to the relaxational contributions from the dipole reversal (flipping) of polar nanoregions and fluctuation of polar region boundaries (breathing), respectively. This behavior is typical in perovskite relaxor ferroelectrics, where the breathing mechanism is present at lower temperature and become the leading contribution when the flipping of the polar regions is frozen-out.[4–6] This two contributions are also observed in relaxor behavior of $Sr_4La_2Ti_4Nb_6O_{30}$, where the high-temperature flipping contribution follows the Vogel-Fulcher law, while the low-temperature breathing contribution shows a Arrhenius behavior.[18] In $Sr_5LaTi_3Nb_7O_{30}$, both the flipping and breathing mechanisms follows well the Vogel-Fulcher law, with the freezing temperature of 189 K (relaxation I) and ~90 K (relaxation II).

As shown in Figure 10, the deviation of lattice parameter c from the linear contraction and increasing of tetragonality (c/a ratio), which are mainly dominated by the c axis, reflect the structure change during the formation of polar nanoregions and the following freezing process of flipping and breathing contributions. However, all the lattice parameters show opposite tendency below 100 K. It seems that the freezing system was disturbed by some low temperature mechanism combined by relaxation III at the same temperature region. Similar dielectric relaxation was observed in strontium barium niobates (SBN) around 100 K, which was more obvious in the dielectric properties along a axis.[35–38] In some compositions, structural phase transition was detected accompanying a polarization tilt from the c axis toward the [110] axis, which was suggested to be the origin of the low-temperature anomalies.[35,36] However, in other compositions, no phase transition was detected and the low temperature relaxation was attributed to some dynamics, which are still active in the ferroelectric phase, like the concerted rotations of the oxygen octahedra.[37,38] In our present study, the phenomena is more close to the latter situation, where no phase transition was observed for $Sr_5LaTi_3Nb_7O_{30}$ ceramics down to 93 K. Therefore, relaxation III is more likely due to the concerted rotations of the oxygen octahedra, which are mainly limited in the ab plane and carried weak dipole moments. This rotation of the oxygen octahedra has also been suggested as the origin of the incommensurate tilted structure in tungsten bronzes.[15,16] Generally, flipping and breathing of polar nanoregions along c axis contribute to the main dielectric relaxation (I and II), while the concerted rotations of the oxygen octahedra in the ab plane dominate relaxation III.

IV. CONCLUSIONS

Correlation of the relaxor nature and crystal structure was studied in lead-free tetragonal tungsten bronze $Sr_5LaTi_3Nb_7O_{30}$ ceramics. The appearance of polar nanoregions was confirmed below the deviation temperature T_D ~330 K, where three dielectric relaxations were observed. Relaxation I and II followed the Vogel-Fulcher law with the freezing temperatures of 189 K and ~90 K, while the low temperature relaxation III followed well the Arrhenius law. Deviation of lattice parameter c from the linear contraction and increasing of tetragonality (c/a ratio) were observed below T_D, reflecting the structure change during the formation of polar nanoregions and the following freezing process. Opposite tendency was observed below 100 K for all the lattice parameters, which corresponds to relaxation III. Flipping and breathing of polar nanoregions along c axis contribute to the main dielectric relaxation (I and II), while the concerted rotations of the oxygen octahedra in the ab plane dominate relaxation III.

ACKNOWLEDGMENTS

The present work was partially supported by National Science Foundation of China under Grant Nos. 51102210 and 51332006. X. L. Zhu acknowledges FCT for financial support (SFRH/BPD/82534/2011).

[1]S. E. Park and T. R. Shrout, J. Appl. Phys. **82**, 1804 (1997).
[2]G. A. Samara, J. Phys.: Condens. Matter **15**, R367 (2003).

[3]A. A. Bokov and Z. G. Ye, J. Mater. Sci. **41**, 31 (2006).
[4]V. Bovtun, J. Petzelt, V. Porokhonskyy, S. Kamba, and Y. Yakymenko, J. Eur. Ceram. Soc. **21**, 1307 (2001).
[5]V. Bovtun, S. Kamba, A. Pashkin, M. Savinov, P. Samoukhina, J. Petzelt, and I. P. Bykov, Ferroelectrics **298**, 23 (2004).
[6]V. Bovtun, S. Veljko, S. Kamba, J. Petzelt, S. Vakhrushev, Y. Yakymenko, K. Brinkman, and N. Setter, J. Eur. Ceram. Soc. **26**, 2867(2006).
[7]P. B. Jamieson, S. C. Abrahams, and J. L. Bernstein, J. Chem. Phys. **48**, 5048 (1968).
[8]A. Simon and J. Ravez, C. R. Chim. **9**, 1268 (2006).
[9]E. O. Chi, A. Gandini, K. M. Ok, L. Zhang, and P. S. Halasyamani, Chem. Mater. **16**, 3616 (2004).
[10]X. M. Chen, Y. Yuan, and Y. H. Sun, J. Appl. Phys. **97**(7), 074108 (2005).
[11]Y. Yuan, X. M. Chen, and Y. J. Wu, J. Appl. Phys. **98**(8), 084110 (2005).
[12]D. C. Arnold and F. D. Morrison, J. Mater. Chem. **19**, 6485 (2009).
[13]A. Rotaru, D. C. Arnold, A. Daoud Aladine, and F. D. Morrison, Phys. Rev. B **83**, 184302 (2011).
[14]S. Kamba, S. Veljko, M. Kempa, M. Savinov, V. Bovtun, P. Vanek, J. Petzelt, M. C. Stennett, I. M. Reaney, and A. R. West, J. Eur. Ceram. Soc. **25**, 3069 (2005).
[15]I. Levin, M. C. Stennett, G. C. Miles, D. I. Woodward, A. R. West, and I. M. Reaney, Appl. Phys. Lett. **89**, 122908 (2006).
[16]M. C. Stennett, I. M. Reaney, G. C. Miles, D. I. Woodward, A. R. West, C. A. Kirk, and I. Levin, J. Appl. Phys. **101**, 104114 (2007).
[17]X. L. Zhu, X. M. Chen, X. Q. Liu, and X. G. Li, J. Mater. Res. **22**(8), 2217 (2007).
[18]V. Bovtun, S. Kamba, S. Veljko, D. Nuzhnyy, K. Knížek, M. Savinov, and J. Petzelt, J. Appl. Phys. **101**, 054115 (2007).
[19]X. L. Zhu, S. Y. Wu, and X. M. Chen, Appl. Phys. Lett. **91**(16), 162906 (2007).
[20]X. L. Zhu, X. M. Chen, and X. Q. Liu, J. Mater. Res. **23**(11), 3112 (2008).
[21]S. R. Shannnigrahi, R. N. P. Choudhary, A. Kumar, and H. N. Acharya, J. Phys. Chem. Solids **59**, 737 (1998).
[22]H. Sharma, K. Kumari, and S. N. Giri, Bull. Mater. Sci. **22**(4), 757 (1999).
[23]P. Ganguly and A. K. Jha, Integr. Ferroelectr. **115**, 149 (2010).
[24]K. Li, X. L. Zhu, X. Q. Liu, and X. M. Chen, Appl. Phys. Lett. **100**, 012902 (2012).
[25]X. L. Zhu, X. Q. Liu, and X. M. Chen, J. Am. Ceram. Soc. **94**(6), 1829 (2011).
[26]J. Rodriguez Carvajal, Comm. Powder Diffr. (IUCr) Newsl. **26**, 12 (2001).
[27]H. X. Yan, F. Inam, G. Viola, H. Ning, H. Zhang, Q. Jiang, T. Zhang, Z. Gao, and M. J. Reece, J. Adv. Dielectr. **1**, 107 (2011).
[28]C. J. Stringer, T. R. Shrout, and C. A. Randall, J. Appl. Phys. **101**, 054107 (2007).
[29]H. Du, W. Zhou, F. Luo, D. Zhu, S. Qu, and P. Pei, J. Appl. Phys. **105**, 124104 (2009).
[30]K. Uchino and S. Nomura, Ferroelectr. Lett. **44**, 55 (1982).
[31]S. M. Pilgrim, A. E. Sutherland, and S. R. Winzer, J. Am. Ceram. Soc. **73**, 3122 (1990).
[32]D. Viehland, S. J. Jang, and L. E. Cross, J. Appl. Phys. **68**, 2916 (1990).
[33]X. L. Zhu, X. M. Chen, and X. G. Li, Appl. Phys. Lett. **90**(18), 182905 (2007).
[34]A. K. Jonscher, *Dielectric Relaxation in Solids* (Chelsea Dielectrics Press, London, 1983).
[35]Y. Xu, Z. Li, W. Li, H. Wang, and H. Chen, Phys. Rev. B **40**, 11902 (1989).
[36]M. Venet, J. de Los, S. Guerra, I. A. Santos, J. A. Eiras, and D. Garcia, J. Phys.: Condens. Matter **19**, 026207 (2007).
[37]J. H. Ko, S. Kojima, S. G. Lushnikov, R. S. Katiyar, T. H. Kim, and J. H. Ro, J. Appl. Phys. **92**, 1536 (2002).
[38]R. R. Neurgaonkar, W. K. Cory, J. R. Oliver, E. J. Sharp, G. L. Wood, M. J. Miller, W. W. Clark, and G. J. Salamo, Mater. Res. Bull. **23**, 1459 (1988).